

Tailoring the nature and strength of electron-phonon interactions in the SrTiO₃(001) two-dimensional electron liquid

Z. Wang,^{1,2} S. McKeown Walker,² A. Tamai,² Y. Wang,^{3,4} Z. Ristic,⁵ F.Y. Bruno,² A. de la Torre,² S. Riccò,² N.C. Plumb,¹ M. Shi,¹ P. Hlawenka,⁶ J. Sánchez-Barriga,⁶ A. Varykhalov,⁶ T.K. Kim,⁷ M. Hoesch,⁷ P.D.C. King,⁸ W. Meevasana,⁹ U. Diebold,¹⁰ J. Mesot,^{1,5,11} B. Moritz,³ T.P. Devereaux,^{3,12} M. Radovic,^{1,13} and F. Baumberger^{2,1,8}

¹*Swiss Light Source, Paul Scherrer Institut, CH-5232 Villigen PSI, Switzerland*

²*Department of Quantum Matter Physics, University of Geneva,
24 Quai Ernest-Ansermet, 1211 Geneva 4, Switzerland*

³*Stanford Institute for Materials and Energy Sciences,
SLAC National Accelerator Laboratory,
Menlo Park, California 94025, USA*

⁴*Department of Applied Physics, Stanford University, Stanford, CA 94305, USA*

⁵*Institute of Condensed Matter Physics,
École Polytechnique Fédérale de Lausanne (EPFL), CH-1015 Lausanne, Switzerland*

⁶*Helmholtz-Zentrum Berlin für Materialien und Energie GmbH*

⁷*Diamond Light Source, Harwell Campus, Didcot, United Kingdom*

⁸*SUPA, School of Physics and Astronomy, University of St Andrews,
St Andrews, Fife KY16 9SS, United Kingdom*

⁹*School of Physics, Suranaree University of Technology,
Nakhon Ratchasima, 30000, Thailand*

¹⁰*Institute of Applied Physics, Vienna University of Technology,
Wiedner Hauptstrasse 8-10/134, A-1040 Vienna, Austria*

¹¹*Laboratory for Solid State Physics,
ETH Zürich, CH-8093 Zurich, Switzerland*

¹²*Geballe Laboratory for Advanced Materials,
Stanford University, Stanford, CA 94305, USA*

¹³*SwissFEL, Paul Scherrer Institut, CH-5232 Villigen PSI, Switzerland*

Surfaces and interfaces offer new possibilities for tailoring the many-body interactions that dominate the electrical and thermal properties of transition metal oxides [1–3]. Here, we use the prototypical two-dimensional electron liquid (2DEL) at the SrTiO₃(001) surface [4–7] to reveal a remarkably complex evolution of electron-phonon coupling with the tunable carrier density of this system. At low density, where superconductivity is found in the analogous 2DEL at the LaAlO₃/SrTiO₃ interface [8–13], our angle-resolved photoemission data show replica bands separated by 100 meV from the main bands. This is a hallmark of a coherent polaronic liquid and implies long-range coupling to a single longitudinal optical phonon branch. In the overdoped regime the preferential coupling to this branch decreases and the 2DEL undergoes a crossover to a more conventional metallic state with weaker short-range electron-phonon interaction. These results place constraints on the theoretical description of superconductivity and allow for a unified understanding of the transport properties in SrTiO₃-based 2DELs.

Carrier concentration is a key parameter defining the ground state of correlated electron systems. At the LaAlO₃/SrTiO₃ interface, the 2DEL density can be tailored by field-effect gating. As the system is depleted of carriers, its ground state evolves from a high mobility 2DEL [4], into a two-dimensional superconductor [8–10] with pseudogap behaviour [11] and possible pairing above T_c [12]. An analogous 2DEL can be induced by doping the (001) surface of SrTiO₃. As for the interface, the surface 2DEL is confined by a band bending potential in SrTiO₃ and consists of an orbitally polarized ladder of quantum confined Ti *t*_{2g} electrons that are highly mobile in the surface plane [5–7, 14]. Thus far, the surface 2DEL has only been studied at carrier densities around 2 × 10¹⁴ cm⁻², approximately a factor of five higher than typically observed at the LaAlO₃/SrTiO₃ interface [5–7]. In the following, we present ARPES data extending to lower carrier densities that are directly comparable to the LaAlO₃/SrTiO₃ interface. We achieve this by preparing SrTiO₃(001) wafers *in situ*, which results in well ordered clean surfaces that can be studied by ARPES over extended timescales as they are less susceptible to the UV induced formation of charged oxygen vacancies reported for cleaved SrTiO₃ [5, 7, 15, 16]. Details of the sample preparation are given in the methods section.

Fig. 1 **a** shows an energy-momentum intensity map for a 2DEL with a carrier density of

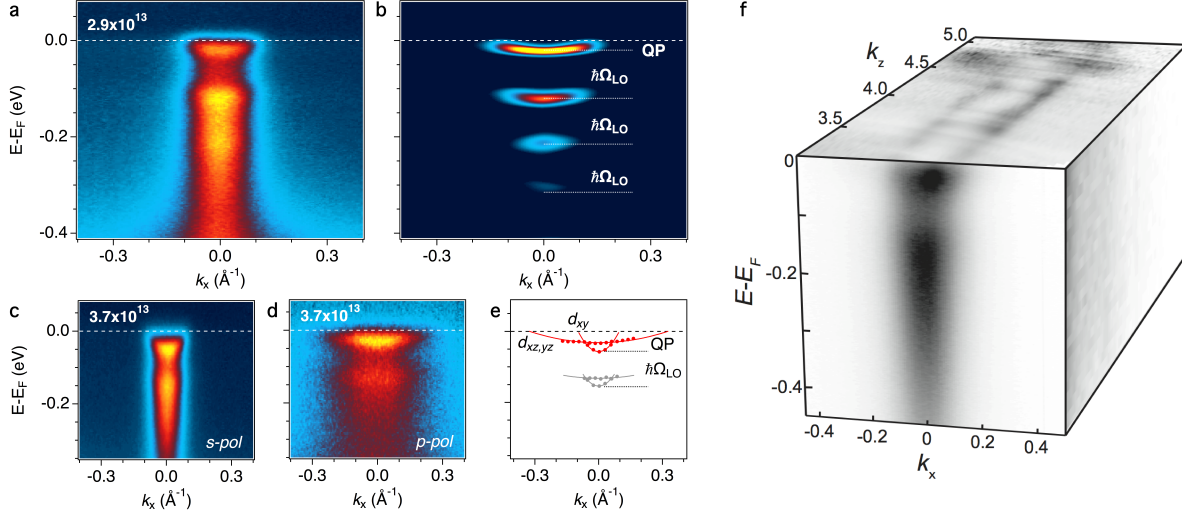


FIG. 1. **A two-dimensional liquid of large polarons in SrTiO₃.** **a,b** Energy-momentum intensity map and curvature plot for a 2DEL with $n_{2D} = 2.9 \cdot 10^{13} \text{ cm}^{-2}$ taken at a photon energy of 44 eV with *s*-polarization. Note the dispersive replica bands at higher binding energy arising from strong coupling to the LO₄ phonon branch of SrTiO₃. **c,d** Data taken on a sample with $n_{2D} = 3.7 \cdot 10^{13} \text{ cm}^{-2}$ using *s* and *p* polarized light with $h\nu = 85 \text{ eV}$ to selectively excite the light *xy* and heavy *xz/yz* orbitals. **e** Dispersion of the main and first replica bands extracted from the data in **c,d**. **f** Photon energy dependent measurements showing the lack of dispersion along k_z . All data were measured in the second Brillouin zone to avoid the minimum of the matrix elements at normal emission.

$n_{2D} \approx 2.9 \cdot 10^{13} \text{ cm}^{-2}$ estimated from the Luttinger volume of the first light subband and the two equivalent heavy subbands (see Supplementary Information section 2). The most striking feature of this data are replica bands at higher binding energy following the dispersion of the primary quasiparticle (QP) bands. The replica bands are all separated by $\approx 100 \text{ meV}$ and progressively loose intensity but can be visualized up to the third replica in the curvature plot shown in Fig. 1 **b**. From the equal energy spacing of the replica bands we can rule out that they represent distinct subbands arising from quantum confinement [5–7, 16]. We thus interpret the replicas as shake-off excitations involving a single non-dispersive bosonic mode coupling electrons of momentum \mathbf{k} and $\mathbf{k} + \mathbf{q}$. From its energy of $\approx 100 \text{ meV}$, we can identify this mode as the highest frequency longitudinal optical phonon branch (LO₄) of SrTiO₃ [17]. A plasmon mode in the same energy range [17, 18] can be excluded from the

negligible density dependence of the mode frequency observed in Fig. 2. Our ARPES data show that the coupling to this mode largely preserves the dispersion in the replica bands and thus must be restricted to small values of \mathbf{q} . This is a hallmark of Fröhlich polarons, quasi-particles formed by an excess electron dressed by a polarization cloud extending over several lattice sites that follows the charge as it propagates through the crystal [2, 19–22]. Such a large polaron state preserves band-like transport but has an increased effective mass m^* . From our ARPES data we can directly quantify this effect. Using a parabolic fit of the band dispersion in Fig. 1 **a** we find $m_{xy}^* \approx 1.4 m_e$. Using a bare band mass of $m_0 = 0.6 m_e$ [7, 15] this corresponds to a mass enhancement $m_{xy}^*/m_0 \approx 2.3$, indicative of an intermediate e - p coupling strength.

In Fig. 1 **c-f** we investigate a sample with slightly higher carrier density. Using s and p polarized light, respectively, we selectively excite electrons from the light xy band with ≈ 50 meV occupied bandwidth and a shallower heavy band derived from xz/yz orbitals. Both bands show a clear peak-dip-hump line shape with a dispersive replica band as summarized in Fig. 1 **e**. This implies that the entire orbitally polarized 2DEL including the heavy xz/yz states, which are believed to be important for superconductivity [9–11], is a polaronic liquid at low carrier densities. The lifting of the orbital degeneracy by approximately 20 meV can be attributed to quantum confinement in the band bending potential which increases the energy of out-of-plane orbitals [7, 23]. The reduced dimensionality arising from quantum confinement is visualized directly in Fig. 1 **f** where we show the absence of dispersion along the surface normal k_z , characteristic of two-dimensional electronic states.

We now turn our attention to the strength of e - p coupling. Its systematic evolution with carrier density in the SrTiO₃(001) 2DEL is shown in Fig. 2. Using s -polarized light, we resolve a single d_{xy} QP band at low density. Energy distribution curves extracted at k_F show a strongly reduced weight of the coherent QP and at least two phonon satellites each separated by ≈ 100 meV. Empirically, we find that the experimental spectra are well described by a Franck-Condon model using a single phonon mode of ≈ 100 meV. Highly restricted fits using the characteristic Poisson distribution $I_n/I_{QP} = a_c^{2n}/n!$ for the intensity ratio of the n -th phonon satellite and the QP peak in the Franck-Condon model are shown in Fig. 2 **g-l**. Details of the fits are described in Supplementary Information. From this analysis we infer a quasiparticle residue $Z \approx 0.2$ at the lowest density studied here. This is beyond the validity of the perturbation theory result for the Fröhlich model of $Z =$

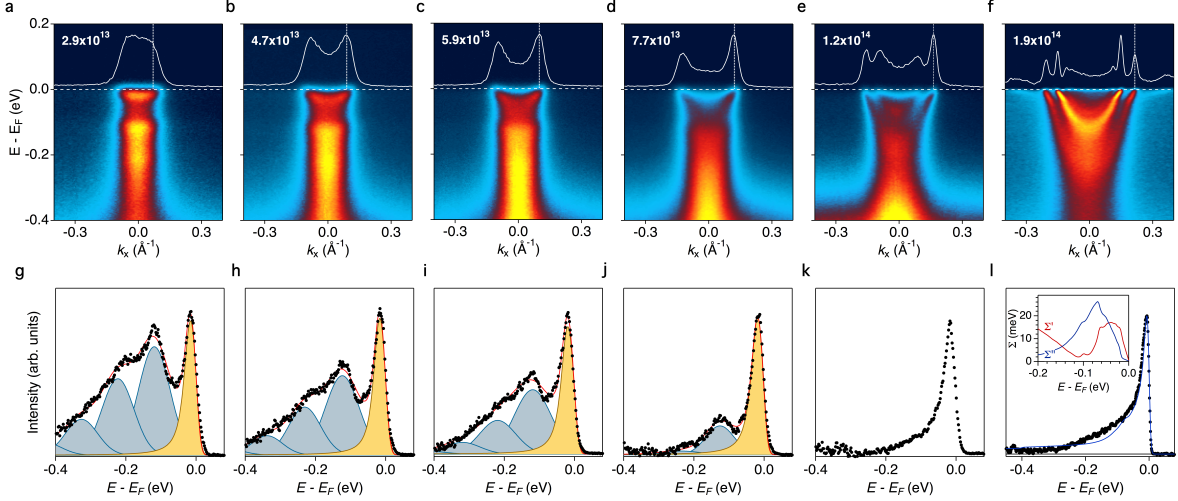


FIG. 2. Evolution of the 2DEL spectral function with carrier concentration. **a-f**, Raw energy-momentum intensity maps of 2DELs with increasing carrier concentration indicated in units of cm^{-2} . **g-l**, Energy distribution curves at the Fermi wave vector indicated by a dashed white line in the corresponding image plots. An exponential background describing the tail of the in-gap state at ≈ -1.1 eV has been subtracted from the raw EDCs (see Supplementary Information). In **g-j** we show fits to a Franck-Condon model with a single phonon mode. The coherent quasiparticle and incoherent phonon satellites are coloured in yellow and blue, respectively. **l** shows a calculation of the spectral function using the conventional Eliashberg e - p self-energy for the high-density limit found in Ref. [7] and reproduced in the inset.

$1 - \alpha/2$ [24, 25], where α is the dimensionless coupling constant, placing the SrTiO₃ 2DEL in a theoretically challenging regime of intermediate coupling. Moreover, the ratio of lattice energy to electron kinetic energy is neither small nor independent of doping, which excludes a Migdal-Eliashberg approach. We therefore estimate α from the experimentally determined quasiparticle residue Z using the results of diagrammatic quantum Monte Carlo simulations of the Fröhlich model reported in Ref. [25]. This gives $\alpha \approx 2.8$ at the lowest carrier density, comparable to $\alpha = 2 - 3$ reported for lightly doped bulk SrTiO₃ based on an analysis of optical conductivity data [26, 27].

As the carrier density increases, the Fermi wave vector increases monotonically, and new subbands become discernible. Concomitantly, the spectral weight of the phonon satellites weakens and for densities above $n_2 \approx 9 \cdot 10^{13} \text{ cm}^{-2}$ they can no longer be resolved experimentally. At high density e - p coupling is not only weaker but also of fundamentally different

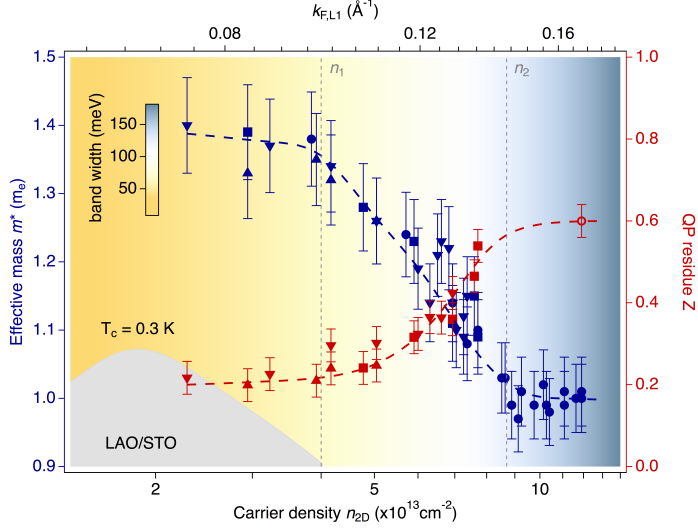


FIG. 3. **Effective mass and quasiparticle residue in the SrTiO₃ 2DEL.** Evolution of the effective mass m^* (blue symbols) and quasiparticle residue Z (red symbols) with carrier density. Different symbols indicate data taken on substrates annealed at different temperature. Closed red symbols are obtained from Franck-Condon fits, while the last value with open symbol in the adiabatic Migdal-Eliashberg regime has been calculated from $Z = m_0/m^*$. Error bars indicate the reproducibility of our results. An additional systematic error cannot be excluded. The background color encodes the bare band width of the first light subband calculated from the experimentally determined k_F shown in the top-axis, assuming a bare mass of $m_0 = 0.6 m_e$. Dashed lines are guides to the eye. The dome shaped superconducting phase observed at the LaAlO₃/SrTiO₃ interface is indicated in grey.

nature. This is illustrated in Fig. 2 **f,l**. In this regime, the quasiparticle dispersion shows a weak kink at an energy of ≈ 30 meV and no signs of replica bands can be discerned in the raw data or in curvature plots (see Supplementary Information, Fig. S4), providing direct evidence for a suppression of the long-range Fröhlich interaction. Instead, consistent with Ref. [7], we find that the spectral function and e - p self-energy of the high-density 2DEL can be described by Migdal-Eliashberg theory with $\lambda \approx 0.7$ and the same coupling to the entire phonon density of states.

In order to track the crossover from the polaronic state to short-range e - p coupling, we analyse the quasiparticle residue and effective mass of the dispersive bands close to the Fermi level as a function of 2D carrier concentration. The results are summarized in

Fig. 3 where we plot m^* obtained from fits to the QP dispersion and $Z(k_F)$ from fits to a Franck-Condon model as described above. Three distinct regimes can be identified. Below $n_1 \approx 4 \cdot 10^{13} \text{ cm}^{-2}$ both quantities depend weakly on carrier density and appear to saturate around $m^* \approx 1.4 m_e$ and $Z(k_F) \approx 0.2$, respectively. At intermediate carrier concentrations of $n_{2D} = 4 - 9 \cdot 10^{13} \text{ cm}^{-2}$, the polaronic state persists, as is seen most directly from the spectra in Fig. 2 **h-j** showing a clear phonon satellite over this entire regime. However, approaching $n_2 \approx 9 \cdot 10^{13} \text{ cm}^{-2}$, where the phonon satellites are no longer resolved experimentally, the quasiparticle residue increases by more than a factor of two to $Z \approx 0.5$ and the effective coupling strength decreases to $\alpha \approx 1.3$. This is opposite to the trend expected for short-range e - p coupling [28] and thus strongly supports our identification of long-range interactions as described by the Fröhlich model. We note that the weak coupling to the LO_4 branch close to n_2 reported in Fig. 3 has recently been confirmed for the $\text{LaAlO}_3/\text{SrTiO}_3$ interface 2DEL in a soft x-ray ARPES study reporting $Z \approx 0.4$ for a sample with $n_{2D} \approx 8 \cdot 10^{13} \text{ cm}^{-2}$, in excellent agreement with our findings [29].

The effective mass decreases more slowly than the quasiparticle residue and saturates at $m^* \approx 1.0 m_e$ at high density. This slow decrease is characteristic of the Fröhlich model where $Z < m_0/m^*$. For weak to intermediate coupling, the effective mass of Fröhlich polarons can be approximated as $m^*/m_0 = 1/(1 - \alpha/6)$ [19, 25]. As shown in Supplementary Information Fig. S6, this relation systematically underestimates the effective masses obtained directly from the quasiparticle dispersion but reproduces their trend as a function of density. We tentatively assign this behavior to the effect of electron-electron interactions, which is not fully included in the analysis of Z in the polaronic regime. Indeed, the factor between the two effective masses is approximately 1.3, which is consistent with the mass-enhancement due to electronic correlations estimated in Ref. [7]. For densities above n_2 , described by Migdal-Eliashberg theory, $Z = m/m^*$ suggesting that the quasiparticle residue saturates around $Z = 0.6$ in the high-density 2DEL.

We attribute the breakdown of the polaronic state at high carrier density to improved electronic screening suppressing the long range Fröhlich interaction. In order to estimate the cross-over from dielectric screening in the polaronic regime to predominantly electronic screening, we compare the polaron radius $r_p = (\hbar/2m^*\Omega_{\text{LO}_4})^{1/2}$ [19] with the electronic screening length. Using the experimentally determined parameters we find $r_p \approx 6 \text{ \AA}$. Given the relatively large dielectric constant of doped SrTiO_3 , electronic screening

is in the Thomas-Fermi regime and the screening length can be estimated from $r_{\text{TF}} = (\epsilon\epsilon_0 E_F / 2e^2 n_{3D})^{1/2}$ for a 3D electron liquid. Assuming a uniform charge distribution over a 2DEL thickness of 3 unit cells and a static dielectric constant $\epsilon_0 = 100$, which provides a good description of the band-bending potential in the doped surface region [7, 16], we estimate that $r_{\text{TF}} = r_p$ for a density $n_{2D} \approx 5 \cdot 10^{13} \text{ cm}^{-2}$, slightly above n_1 where Z starts to increase progressively resulting in a reduced effective coupling constant α . At higher carrier densities, electronic screening will rapidly become more important as ϵ_0 decreases simultaneously with the increase in n . We note that the moderate electronic screening length r_{TF} justifies the above use of an expression for 3D electron liquids. This basic picture is consistent with the temperature dependence of the electron mobility in SrTiO₃ 2DELs [30] and further confirmed by our calculations of the spectral function reported in supplementary Fig. S5. Using exact diagonalization of a model Hamiltonian with constant coupling parameter, we find pronounced replica bands at low carrier density and a rapid suppression of the replicas as the carrier density is increased over the relevant range. These calculations thus reproduce the key experimental findings of our study and support the idea that increasing electronic screening drives the observed breakdown of the polaronic liquid at high carrier densities.

The above results demonstrate that e - p interaction in SrTiO₃ based 2DELs is remarkably complex and strongly dependent on carrier density. This provides insight into the superconducting pairing mechanism at the LaAlO₃/SrTiO₃ interface, which has so far eluded experimental investigation. As shown in Fig. 3, superconductivity in LaAlO₃/SrTiO₃ interface 2DELs [8–10, 31] occurs in the polaronic low-density regime and its suppression on the overdoped side coincides with a gradually decreasing coupling to the LO₄ branch. This supports the notion that superconductivity is phonon mediated [13, 32, 33] and suggests that the pairing potential is dominated by the exchange of high-frequency longitudinal phonons rather than soft modes. We note that our experimental spectral functions do not exclude the formation of large bipolarons, which have been discussed early on in the context of superconductivity in polar oxides [34, 35]. Superconducting susceptibilities calculated within our exact diagonalization scheme reported in supplementary information section 5 provide additional insight. Although limitations in the Hilbert space size prohibit a quantitative comparison with experiment, the calculations clearly show that the dominant pairing channel has s -wave symmetry. Moreover, the saturation of the superconducting suscepti-

bility with carrier density found in this model provides evidence for a competition between the opposite trends of density of states and effective e - p coupling underlying dome-shaped superconductivity in SrTiO₃ 2DELs. We note that coupling to the LO₄ branch of SrTiO₃ with comparable strength was also invoked to explain the anomalously high superconducting critical temperature of FeSe monolayers on SrTiO₃ substrates [2, 36].

-
- [1] Mannhart, J. & Schlom, D. G. Oxide interfaces—an opportunity for electronics. *Science* **327**, 1607–1611 (2010).
 - [2] Lee, J. J. *et al.* Interfacial mode coupling as the origin of the enhancement of T_c in FeSe films on SrTiO₃. *Nature* **515**, 245–248 (2014).
 - [3] Zubko, P., Gariglio, S., Gabay, M., Ghosez, P. & Triscone, J.-M. Interface physics in complex oxide heterostructures. *Annu. Rev. Condens. Matt. Phys.* **2**, 141–165 (2011).
 - [4] Ohtomo, A. & Hwang, H. Y. A High-mobility Electron Gas at the LaAlO₃/SrTiO₃ Heterointerface. *Nature* **427**, 423–426 (2004).
 - [5] Meevasana, W. *et al.* Creation and control of a two-dimensional electron liquid at the bare SrTiO₃ surface. *Nat. Mater.* **10**, 114–118 (2011).
 - [6] Santander-Syro, A. F. *et al.* Two-dimensional Electron Gas with Universal Subbands at the Surface of SrTiO₃. *Nature* **469**, 189–193 (2011).
 - [7] King, P. D. C. *et al.* Quasiparticle dynamics and spin-orbital texture of the SrTiO₃ two-dimensional electron gas. *Nat. Commun.* **5**, 3414 (2014).
 - [8] Thiel, S., Hammerl, G., Schmehl, A., Schneider, C. W. & Mannhart, J. Tunable Quasi-Two-Dimensional Electron Gases in Oxide Heterostructures. *Science* **313**, 1942–1945 (2006).
 - [9] Reyren, N. *et al.* Superconducting Interfaces Between Insulating Oxides. *Science* **317**, 1196–1199 (2007).
 - [10] Caviglia, A. D. *et al.* Electric field control of the LaAlO₃/SrTiO₃ interface ground state. *Nature* **456**, 624–627 (2008).
 - [11] Richter, C. *et al.* Interface superconductor with gap behaviour like a high-temperature superconductor. *Nature* **502**, 528–531 (2008).
 - [12] Cheng, G. *et al.* Electron pairing without superconductivity. *Nature* **521**, 196–199 (2015).
 - [13] Boschker, H., Richter, C., Fillis-Tsirakis, E., Schneider, C. W. & Mannhart, J. Electron—

- phonon Coupling and the Superconducting Phase Diagram of the LaAlO₃-SrTiO₃ Interface. *Sci. Rep.* **5**, 12309 (2015).
- [14] Plumb, N. C. *et al.* Mixed Dimensionality of Confined Conducting Electrons in the Surface Region of SrTiO₃. *Phys. Rev. Lett.* **113**, 086801 (2014).
- [15] Wang, Z. *et al.* Anisotropic Two-dimensional Electron Gas at SrTiO₃(110). *Proc. Natl. Acad. Sci. U.S.A.* **111**, 3933–3937 (2014).
- [16] McKeown Walker, S. *et al.* Carrier-Density Control of the SrTiO₃ (001) Surface 2D Electron Gas studied by ARPES. *Adv. Mater.* **27**, 3894–3899 (2015).
- [17] Gervais, F., Servoin, J.-L., Baratoff, A., Bednorz, J. G. & Binnig, G. Temperature dependence of plasmons in Nb-doped SrTiO₃. *Phys. Rev. B* **47**, 8187–8194 (1993).
- [18] Chang, Y. J., Bostwick, A., Kim, Y. S., Horn, K. & Rotenberg, E. Structure and correlation effects in semiconducting SrTiO₃. *Phys. Rev. B* **81**, 235109 (2010).
- [19] Devreese, J. T. & Alexandrov, A. S. Fröhlich polaron and bipolaron : recent developments. *Rep. Prog. Phys.* **72**, 066501 (2009).
- [20] Alexandrov, A. S. *Theory of Superconductivity: From Weak to Strong Coupling*. Series in Condensed Matter Physics (Institute of Physics, 2003).
- [21] Moser, S. *et al.* Tunable Polaronic Conduction in Anatase TiO₂. *Phys. Rev. Lett.* **110**, 196403 (2013).
- [22] Chen, C., Avila, J., Frantzeskakis, E., Levy, A. & Asensio, M. C. Observation of a two-dimensional liquid of Fröhlich polarons at the bare SrTiO₃ surface. *Nat. Commun.* **6**, 8585 (2015).
- [23] Salluzzo, M. *et al.* Orbital Reconstruction and the Two-Dimensional Electron Gas at the LaAlO₃/SrTiO₃ Interface. *Phys. Rev. Lett.* **102**, 166804 (2009).
- [24] Lee, T. D., Low, F. E. & Pines, D. The motion of slow electrons in a polar crystal. *Phys. Rev.* **90**, 297–302 (1953).
- [25] Mishchenko, A. S., Prokof'ev, N. V., Sakamoto, A. & Svistunov, B. V. Diagrammatic quantum Monte Carlo study of the Fröhlich polaron. *Phys. Rev. B* **62**, 6317–6336 (2000).
- [26] van Mechelen, J. L. M. *et al.* Electron-Phonon Interaction and Charge Carrier Mass Enhancement in SrTiO₃. *Phys. Rev. Lett.* **100**, 226403 (2008).
- [27] Devreese, J. T., Klimin, S. N., van Mechelen, J. L. M. & van der Marel, D. Many-body large polaron optical conductivity in SrTi_{1-x}Nb_xO₃. *Phys. Rev. B* **81**, 125119 (2010).

- [28] Mishchenko, A. S., Nagaosa, N. & Prokof'ev, N. Diagrammatic Monte Carlo Method for Many-Polaron Problems. *Phys. Rev. Lett.* **113**, 166402 (2014).
- [29] Cancellieri, C. *et al.* Polaronic metal state at the LaAlO₃/SrTiO₃ interface. *Nat. Commun.* **7** (2016).
- [30] Mikheev, E. *et al.* Limitations to the room temperature mobility of two- and three-dimensional electron liquids in SrTiO₃. *Appl. Phys. Lett.* **106**, 062102 (2015).
- [31] Lin, X. *et al.* Critical Doping for the Onset of a Two-Band Superconducting Ground State in SrTiO_{3- δ} . *Phys. Rev. Lett.* **112**, 207002 (2014).
- [32] Klimin, S. N., Tempere, J., Devreese, J. T. & van der Marel, D. Interface superconductivity in LaAlO₃/SrTiO₃. *Phys. Rev. B* **89**, 184514 (2014).
- [33] Gorkov, L. P. Phonon Mechanism in the Most Dilute Superconductor : n-type SrTiO₃. *arXiv:1508.00529* (2015).
- [34] Emin, D. Formation, motion, and high-temperature superconductivity of large bipolarons. *Phys. Rev. Lett.* **62**, 1544–1547 (1989).
- [35] Hohenadler, M., Aichhorn, M. & Von Der Linden, W. Single-particle spectral function of the Holstein-Hubbard bipolaron. *Phys. Rev. B* **71**, 12 (2004).
- [36] Wang, Q.-Y. *et al.* Interface-Induced High-Temperature Superconductivity in Single Unit-Cell FeSe Films on SrTiO₃. *Chinese Phys. Lett.* **29**, 037402 (2012).

Methods The Nb-doped (0.5 wt%) and La-doped (0.075 wt%) SrTiO₃(001) surfaces were prepared by mild Ar⁺ sputtering (600 eV, 2 μ A, 5 min) followed by annealing in $2 \cdot 10^{-6}$ mbar oxygen for 0.5 h at temperatures varying from 700 to 1000°C as monitored by an infrared pyrometer. Consistent with measurements on *in situ* prepared and cleaved SrTiO₃, we find no spectral weight in the entire bulk band gap on freshly prepared surfaces (see Supplementary Information, Fig. 1) [5, 15, 16]. Quantum confined metallic states appear concomitant with a localized in-gap state at higher energy after exposure of the surface to synchrotron light [5, 15, 16]. We find that the rate at which the 2DEL carrier density increases under the synchrotron beam increases with the annealing temperature and exploit this to stabilize low-carrier densities over the extended exposure times required for detailed ARPES measurements. ARPES measurements were performed at the SIS beamline of the Swiss Light Source, the I05 beamline of Diamond Light Source and the 1² beamline of BESSY II at the Helmholtz-Zentrum Berlin. Data was acquired at $T \approx 20$ K with $h\nu = 30 - 100$ eV and

energy and angular resolutions of 10 – 25 meV and $\approx 0.2^\circ$, respectively.

Acknowledgments We thank A. Fête, M. Grilli, L. Patthey, V. Strocov, J.-M. Triscone, D. van der Marel and Z. Zhong for discussions. The ARPES work was supported by the Swiss National Science Foundation (200021-146995). The spectral function calculations were supported at SLAC and Stanford University by the U.S. Department of Energy, Office of Basic Energy Sciences, Division of Materials Sciences and Engineering, under Contract No. DE-AC02-76SF00515 and by the Computational Materials and Chemical Sciences Network (CMCSN) under Contract No. DE-SC0007091. A portion of the computational work was performed using the resources of the National Energy Research Scientific Computing Center supported by the U.S. Department of Energy, Office of Science, under Contract No. DE-AC02-05CH11231. PDCK was supported by the UK-EPSRC (EP/I031014/1) and the Royal Society, UD by the ERC Advanced Grant 'OxideSurfaces' and WM by the Thailand Research Fund (TRF) under the TRF Senior Research Scholar, Grant No. RTA5680008. We acknowledge Diamond Light Source for time on beamline I05 under proposal SI11741.

Author contributions ARPES measurements were carried out by ZW, SMW, ZR, FYB, AdlT, SR, MR and FB and analyzed by ZW, AT and FB. NCP, MS, PH, JSB, AV, TKK and MH were responsible for the synchrotron beam lines used in the experiments. YW, BM and TPD performed the exact diagonalization calculations. FB wrote the manuscript with contributions by ZW, YW, and AT. All authors contributed to the scientific discussion of the results.